

We are IntechOpen, the world's leading publisher of Open Access books Built by scientists, for scientists

4,800

Open access books available

122,000

International authors and editors

135M

Downloads

Our authors are among the

154

Countries delivered to

TOP 1%

most cited scientists

12.2%

Contributors from top 500 universities



WEB OF SCIENCE™

Selection of our books indexed in the Book Citation Index
in Web of Science™ Core Collection (BKCI)

Interested in publishing with us?
Contact book.department@intechopen.com

Numbers displayed above are based on latest data collected.
For more information visit www.intechopen.com



Biomechanics and FE Modelling of Aneurysm: Review and Advances in Computational Models

Simona Celi and Sergio Berti

Additional information is available at the end of the chapter

<http://dx.doi.org/10.5772/46030>

1. Introduction

Abdominal aortic aneurysm (AAA) disease is the 18th most common cause of death in all individuals and the 15th most common in individuals aged over 65 [48]. Clinical treatment for this disorder can consist of open surgical repair or, more recently, of minimally invasive endovascular repair procedures [71]. However, both clinical treatments present significant risks and, consequently, require specific patient selection. Given the risks of current repair techniques, during the course of an aneurysm it is important to determine when the risk of rupture justifies the risk of repair. In this scenario, how to determine the rupture risk of an aneurysm is still an open question. Currently, the trend in determining the severity of an AAA is to use the maximum diameter criterion. Unfortunately, this criterion is only a general rule and not a reliable indicator since small aneurysms can also rupture, as reported in autopsy studies, while many aneurysms can become very large without rupturing [16]. The maximum diameter criterion, in fact, is based on the law of Laplace that establish a linear relationship between diameter and wall stress. However, the law of Laplace is simply based on cylindrical geometries, where only one radius of curvature is involved, whereas aneurysms are complex structures, and therefore the law fails to predict realistic wall stresses. From a biomechanical point of view, rupture events occur when acting wall stresses exceed the tensile strength of the degenerated aortic abdominal (AA) wall. Biomechanics relates the function of a physiological system to its structure and its objective is to deduce the function of a system from its geometry, material properties and boundary conditions based on the balance laws of mechanics (e.g. conservation of mass, momentum and energy). Consequently, from a more general and extensive perspective, the stress state in a body is determined by several factors such as geometry, material properties, load and boundary conditions. In order to understand the capability to estimate the potential rupture risk, it is fundamental to capture the mechanical response of the aortic tissue and its changes during aneurysmal formation. In fact, while, to date, the precise pathogenesis of AAA is poorly understood, it is well known that this change significantly impact on the structure of the aortic wall and on its mechanical behavior.

This chapter will review the state of literature on the mechanical properties and modelling of AAA tissue and will present advanced computational models. The first part (Sec. 2) includes a description of the mechanical test currently used (2.1), the aortic mechanical properties (2.2) and a review of the literature on material constitutive equations (2.3) and geometrical models (2.4). To stress out the morphological complexity of the aortic segment, in Sec 3 the regional variations of material properties and wall thickness reported in literature from experimental investigations are reported. The second part (Sec. 4) describes our original contribution with a description of our Finite Element (FE) models and our probabilistic approach implemented into FE simulations to perform sensitivity analysis (Sec. 4.1). The main results are reported in Sec. 4.2 and discussed in detail in Sec. 5.

2. Review

In order to understand the biomechanical issues in the etiology and treatment of abdominal aortic aneurysms, it is important to understand the structures of the aortic wall and how they affect the mechanical response. Biological tissues are subject to the same balance laws of conservation of mass, momentum and energy of the classical engineering material. What distinguish biological tissues from materials of the field of classical engineering mechanics is their unique structure. Soft biological tissues, in fact, have a very complex structure that can be regarded as either *active* and *passive*. The active components arise from the activation of the smooth muscle cells while the passive response is governed primarily by the elastin and collagen fibres [15]. The distribution and the arrangement of the collagen fibres, in particular, have a significant influence on the mechanical properties due to they attribute anisotropic properties [49] to the tissue. Different studies have shown that this structural arrangement is very complex and varies according to the aortic segment (thoracic or abdominal) [20]. As well as being anisotropic, the material response of soft biological tissue is also highly non-linear.

2.1. Experimental test

To determine mechanical properties of AAA, studies have used both *in-vivo* "tests" and *ex-vivo/in-vitro* testing. As reported by Raghavan and da Silva [53], both of them offer advantages and disadvantages. In particular, in the first case the main difficult is to accurately determine the true force and the displacement distribution ascertaining stress-free configuration of the biological entity. On the other side, isolating samples may introduce as yet unknown changes to their behavior affecting the results of such tests. *In vivo* measurement are often performed by using imaging modality. By using ultrasound phase-locked echo-tracking, Lanne et al. [43] reported that the pressure-strain elastic modulus (E_p), Eq. 1, was higher on average and more widely dispersed in aneurysmal abdominal aorta compared to the non-aneurysmal aorta group. The E_p modulus was calculated based on the diameter (D_s, D_d) and pressure (P_s, P_d) at the systolic and diastolic values as follow:

$$E_p = D_p \frac{P_s - P_d}{D_s - D_d} \quad (1)$$

Using similar consideration, MacSweeney et al. [44] founded that E_p was higher in aneurysmal abdominal aorta compared to controls.

More recently, van't Veer et al. [75] estimated the compliance and distensibility of the AAA by means of simultaneous instantaneous pressure and volume measurements obtained with the

magnetic resonance imaging (MRI). By using time resolved ECG-gated CT imaging data from 67 patients, Ganten et al. [27] found that the compliance of AAA did not differ between small and large lesions. In 2011 Molacek and co-authors [47] did not find any correlation between aneurysm diameter and distensibility of AAA wall and of normal aorta. However it is worth to notice that all these studies do not provide intrinsic mechanical properties of the tissue but more general extrinsic AAA behavior. As far as the *ex-vivo* testing, there are several types of mechanical tests that can be carried out on materials to obtain information on their mechanical behavior. Such tests include simple tension test, biaxial tension, conducted on thin samples of material, and extension/inflation test of thin-walled tubes.

Uniaxial test. Uniaxial extension testing is the simplest and most common of *ex-vivo* testing methods. Here, a rectangular planar sample is subjected to extension along its length at a constant displacement (or load) rate while the force (or the displacement) is recorded during extension. Under the assumption of incompressibility (zero changes of volume during the tensile test, Eq. 2) the recorded force-extension data are converted to stress/strain:

$$A_0 L_0 = AL \quad (2)$$

where A_0 and L_0 are the initial cross sectional area and the initial length while A and L are the values in the current configuration. Interested reader can refer to Di Puccio et al. [19] for a recent review on the incompressibility assumption on soft biological tissue.

Biaxial test. Due to the presence of the collagen fibers, the uniaxial testing is not sufficient for highlighting the aorta tissue and the stress distribution does not fully conform to physiological conditions. Therefore, biaxial tension tests should be performed. During biaxial test, an initial square thin sheet of material is stress normally to both edges. Even if, theoretically, the biaxial test are not sufficient to fully characterized anisotropic materials, [40, 50] they are able to capture additional information regarding the mechanical behavior of the specimens with respect to uniaxial one. By contrast, biaxial tests provides a complete characterization of the material properties for isotropic material. To some extent soft biological tissues can be considered as isotropic within certain limitation, however, in their general formulation, they respond anisotropically under loads. Figure 1 depicts as example the mechanical test and response of a soft tissue under uniaxial (a) and biaxial (b) test.

As we can observe, a distinctive mechanical characteristic of soft tissue in tension tests is its initial flat response and relatively large extensions followed by an increased stiffening at higher extension. As it is well known, this behavior is the result of collagen fibres recruitment as proposed by Roach and Burton [61]. The non-linear stress strain curve arises from the phenomenon of the fibres recruitment. As the material is stretched, the fibres gradually become uncrimped and become more aligned with the direction of applied load.

The results of uniaxial and biaxial tests are used to characterize the mechanical behavior of soft tissue under investigation. Due to the large deformation that characterizes this type of tissue, from a mathematical point of view, a Strain Energy Function (SEF) denoted by W is introduced. The Cauchy stress tensor (σ) is calculated as:

$$\sigma = J^{-1} \mathbf{F} \frac{\partial W}{\partial \mathbf{F}} \quad (3)$$

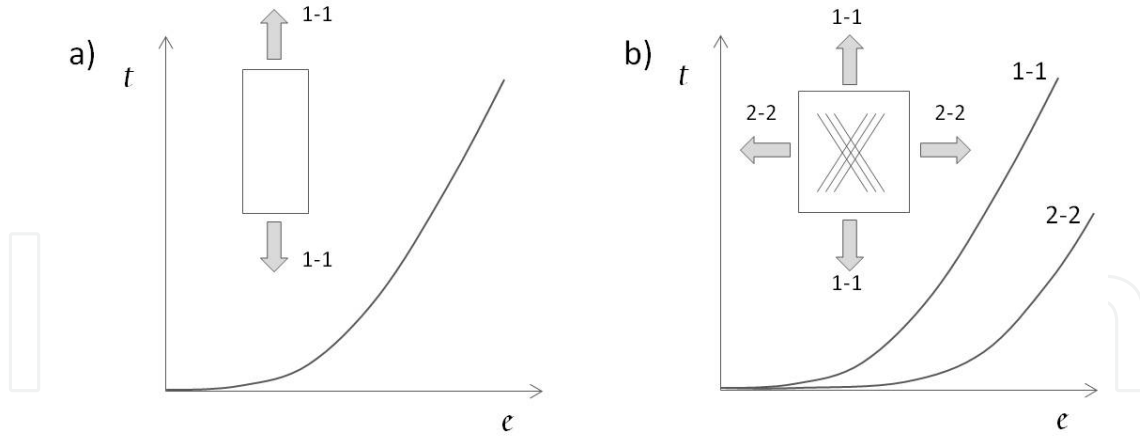


Figure 1. Schematic of uniaxial (a) and biaxial (b) test and curves. The t value is a representative tension value and e a typical extension dimension.

where \mathbf{F} is the deformation gradient tensor, defined as $\mathbf{F} = \partial \mathbf{x} / \partial \mathbf{X}$, i.e. the derivative of the current position \mathbf{x} as regards to the initial position \mathbf{X} during a deformation process and J is the determinant of \mathbf{F} . Under the assumption of incompressibility ($J=1$), the SEF is split in a volumetric (W_{vol}) and isochoric (W_{isoch}) component. In case of uniaxial test we have:

$$\sigma_{11} = \lambda_{11} \frac{\partial W_{isoch}}{\partial \lambda_{11}} \quad (4)$$

where λ_{11} is the stretch in the 1-1 direction (see Fig. 1 (a)). For biaxial test both components can be calculated:

$$\sigma_{\theta\theta} = \lambda_{\theta\theta} \frac{\partial W_{isoch}}{\partial \lambda_{\theta\theta}} \quad (5)$$

$$\sigma_{zz} = \lambda_{zz} \frac{\partial W_{isoch}}{\partial \lambda_{zz}} \quad (6)$$

Equations 5-6 represent the stress components used in the follow sections. With respect to Fig. 1 direction 1-1 and 2-2 are now defined as the circumferential $\sigma_{\theta\theta}$ and the axial σ_{zz} ones, respectively.

2.2. Mechanical properties of healthy and pathological aortic tissue

AAA development is multifactorial phenomenon. A mechanism postulated for AAA formation focuses on inflammatory processes where macrophages recruitment leads to MMP production and elastase release. The biomechanical change associated with enzymatic degradation of structural proteins suggests that AAA expansion is primarily related to elastolysis [21]: a decreasing quadratic relationship was found between elastin concentration and diameter for normal aortas and for pathological increasing diameter [65]. Despite universal recognition of the importance of wall mechanics in the natural history of AAAs [2, 38, 81], there are few detailed studies of the mechanical properties.

Early studies focused on simple uniaxial tests. He and Roach [32] obtained rectangular specimen strips during surgical resection of eight AAA patients and subjected them to uniaxial extension tests up to a pre-defined maximum load rather than until failure. They showed that the stress-strain behavior of AAA tissue was non-linear. Later, in two reports,

Vorp et al. [82] and Raghavan et al. [57] reported on uniaxial extension testing of strips harvested from the anterior midsection of 69 AAA. The specimens were extended until failure. In most cases, the rectangular specimens' length was in the axial orientation, but in a small population, they were oriented circumferentially. Results have found that aneurysmal tissue is substantially weaker and stiffer than normal aorta [18, 57, 70].

To date, the most complete data on both the biaxial mechanical behavior of aorta and AAAs comes from Vande Geest et al. [76, 77]. The source of these specimens becomes from AAA ventral tissue available during the open surgical repair of unruptured lesions. They reported biaxial mechanical data for AAA (26 samples) and normal human AA as a function of age: less than 30, between 30 and 60 and over 60 years of age. In particular Vande Geest and co-workers confirmed that the aortic tissue becomes less compliant with age and that AAA tissue is significantly stiffer than normal abdominal aortic tissue, Figure 2.

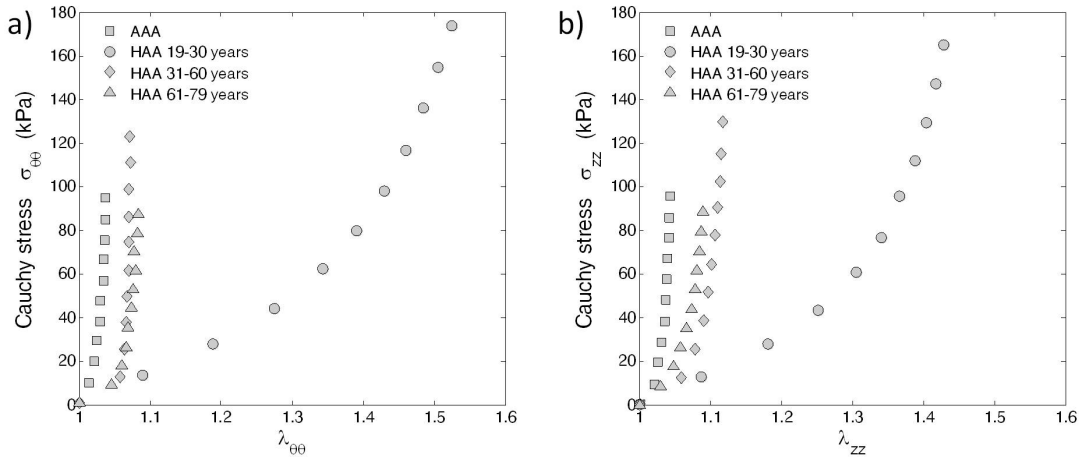


Figure 2. Stress-stretch plot comparing the equibiaxial response for AAA and HAA for four patient groups, for circumferential direction (a) and axial direction (b). Modified from [22].

The specimen was subjected to force-controlled testing with varying prescribed forces between the two orthogonal directions. A CCD camera was used to track the displacement of markers forming a 5x5 mm square placed on the specimen. It is worth to stress out that the use of optical extensometer (markers tracking with CCD camera) is fundamental to measure the deformation during test avoiding the potential tissue slippage from the clamps. Figure 3 depicts a representative biaxial stress-stretch data for healthy (a-b) and pathological (c-d) samples considering three different tension ratios ($T_\theta : T_z$) equal to 1:1, 0.75:1 and 1:0.75.

2.3. Material models

Equations that characterize a material and its response to applied loads are called constitutive relations since they describe the gross behavior resulting from the internal constitution of a material. Constitutive modelling of vascular tissue is an active field of research and numerous descriptions have been reported. Constitutive models for biological tissues can be established following a so-called phenomenological or structural approach. The first type of formulation [14, 26, 36, 73] does not take into account any histological constituents and attempt to describe the global mechanical behavior of the tissue without referring to its underlying microstructure. The phenomenological approach is commonly used but has led to a number of difficulties in describing the mechanical behavior of tissues. Among phenomenological

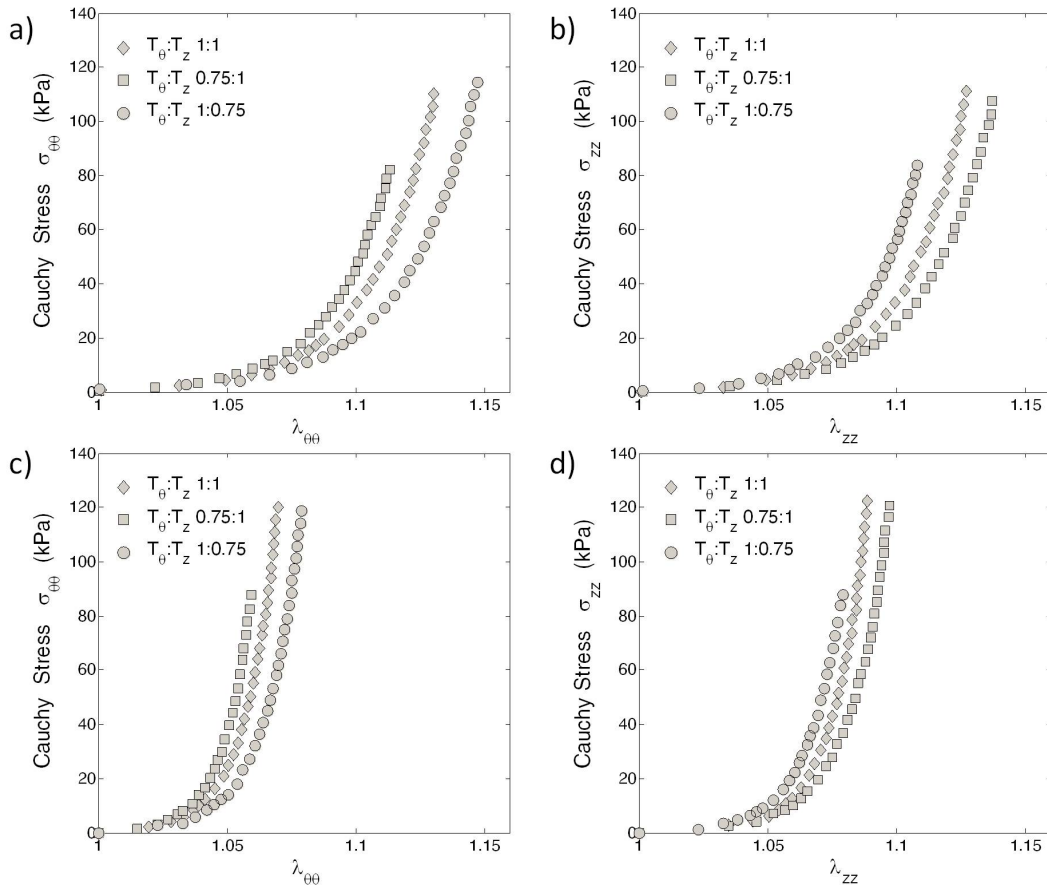


Figure 3. Experimental biaxial data for both healthy (a-b) and pathological (c-d) samples with different tension ratio. Open diamonds, 1 : 1; open squares, 0.75 : 1 and open circles, 1 : 0.75. Modified from [9].

SEFs, Vande Geest and co-authors [77] found that a constitutive functional form used earlier by Choi and Vito [12], Equation 7, would best suit their experimental data:

$$W_{isoch} = b_0 \left(e^{\frac{1}{2}b_1 E_{\theta\theta}^2} + e^{\frac{1}{2}b_2 E_{zz}^2} + e^{\frac{1}{2}b_3 E_{\theta\theta} E_{zz}} - 3 \right) \quad (7)$$

where b_0 , b_1 , b_2 and b_3 are the material parameters and $E_{\theta\theta}$ and E_{zz} are the components of the Green-strain tensor (Eq. 8) defined as follows:

$$\mathbf{E} = \frac{1}{2} (\mathbf{C} - \mathbf{I}) = \frac{1}{2} (\mathbf{F}\mathbf{F}^T - \mathbf{I}) \quad (8)$$

where \mathbf{I} is the identity matrix and \mathbf{C} is the right Cauchy-Green strain tensor.

Alternatively, structural constitutive descriptions [5, 28, 34, 35] overcome this limitation and integrate histological and mechanical information of the arterial wall. In particular, the contributions of constitutive cells, fibers and networks of elements are added together to depict the whole tissue behavior. The structural-based approach has become common with the advent of microstructural imaging methods [64, 80]. In fact, soft biological tissues have a very complex microstructure, consisting of many different components and including elastin fibres, collagen fibres, smooth muscle cells and extracellular matrix.

The same experimental data obtained by vande Geest et al. [77] were then fitted by using an invariant based constitutive equation with two fibre families (2FF) by Basciano et al. [5], Eq.

9, and Rodriguez et al. [62, 63], Eq. 10.

$$W_{isoch} = \alpha (\bar{I}_1 - 3)^2 + \beta (\bar{I}_4 - 1)^6 + \gamma (\bar{I}_6 - 1)^6 \quad (9)$$

$$W_{isoch} = C_1 (\bar{I}_1 - 3) + \sum_{i=3}^4 \frac{k_1^i}{2k_2^i} \left(e^{k_2^i ((1-\rho)(\bar{I}_1-3)^2 + \rho(\bar{I}_4-I_0)^2)} - 1 \right) \quad (10)$$

where \bar{I}_1 is the first invariant of the isochoric portion of the right Cauchy-Green stretch tensor (Eq. 11) and \bar{I}_4 and \bar{I}_6 are mixed invariants of the isochoric portion of the right Cauchy-Green deformation tensor (Eq. 12-13), introduced from embedded fibers [6, 33, 69].

$$\bar{I}_1 = tr \bar{\mathbf{C}} \quad (11)$$

$$\bar{I}_4 = \mathbf{a}_0 \cdot \bar{\mathbf{C}} \mathbf{a}_0 \quad (12)$$

$$\bar{I}_6 = \mathbf{b}_0 \cdot \bar{\mathbf{C}} \mathbf{b}_0 \quad (13)$$

where \mathbf{a}_0 , \mathbf{b}_0 are the direction of the fibers as reported in Figure 4(a-b). In Eq. 9, α is the coefficients for the isotropic part while β and γ for the anisotropic component. In the same manner, in Eq. 10, C_1 is a stress-like material parameter for the purely elastin contribute, and k_j^i are material parameters corresponding to the fibers ($k_1^3 = k_1^4$ and $k_2^3 = k_2^4$). The parameter $\rho \in [0;1]$ is a (dimensionless) measure of anisotropy, $I_0 > 1$ is dimensionless parameters regarded as the initial crimping of the fibers (Fig. 4(b)).

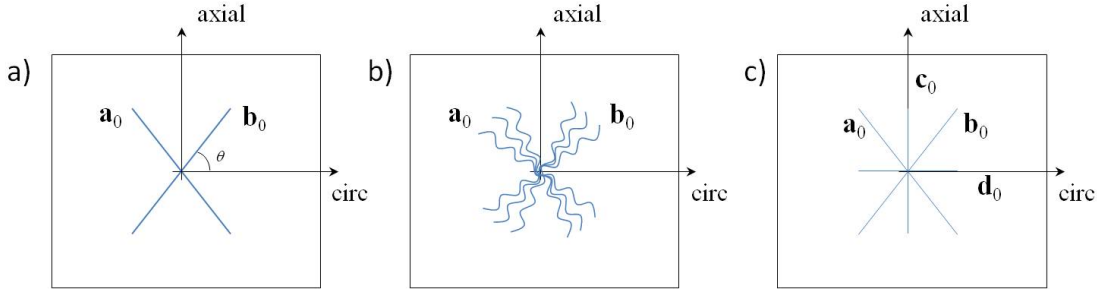


Figure 4. Collagen fiber orientation (\mathbf{a}_0 , \mathbf{b}_0) in a square specimen of tissue for the 2FF model (a), the 2FF model with dispersion (b) and for the 4FF model (c). Note the crimp and fibres dispersion in case (b) and the two additional fibre family (\mathbf{c}_0 , \mathbf{d}_0) in (c).

A constitutive relation based on four fibres family (4FF) (Fig. 4(c)) was proposed by Baek et al. [4], including two additionally fibres family (in longitudinal and circumferential direction, [86]), Equation 14:

$$W_{isoch} = \frac{c}{2} (\bar{I}_1 - 3) + \sum_{i=1}^4 \frac{c_1^i}{4c_2^i} \left(e^{c_2^i (\bar{I}_4^i - 1)^2} - 1 \right) \quad (14)$$

where c , c_1^i and c_2^i are material parameters for this specific SEF. Ferruzzi et al. [22] assumed that diagonal families of collagen were regarded as mechanically equivalent, hence $c_1^3 = c_1^4$, $c_2^3 = c_2^4$. By fitting the biaxial data, the model parameter associated with the isotropic term decreased with increasing age for AA specimens and decreased markedly for AAA specimens [22, 31]. These finding are in good agreement with histopathological results of reduced elastin in ageing [30, 51] and AAAs, e.g. [32, 60].

For all models, the diagonal fibres are accounted for by $\mathbf{a}_0 = -\mathbf{b}_0$; in the 4FF model, axial (\mathbf{c}_0) and circumferential (\mathbf{d}_0) fibres are fixed at 90° and 0° , respectively.

Among the variety of constitutive equations reported in literature, the most significant difference in structural formulation were included by Holzapfel group [62] and by Baek and co-authors [4]. For a more detailed analysis on the effect of this assumption and a comparison between the two constitutive model, interested reader can refer to [17]. It is worth to stress out that, as observed by Zeinali-Davarani and co-authors [87], in parameter estimation, the larger number of parameters for a model provides more flexibility and generally gives better fitting, i.e., decreases the residual error. A common assumption in all previous models is to assume the same fibers distribution and mechanical response throughout the thickness. More recently Schriefl et al. [66] has observed that in the case of the intima layer, due to the higher fibers dispersion, the number of fiber families varying from two to four. However, not all intimas investigated had more than two fiber families while two prominent fibers families were always visible. The number of fiber families equal to two was previously reported by Haskett et al. [31] by analyzing 207 aortic samples.

Finally, it is worth to notice that it is fundamental to define a constitutive model and its material constants over some specific range, from experiments that replicate conditions (physiological or pathological), [17], in order to provide more accurate response. In fact all constitutive formulation are based on specific assumptions and hypotheses. The complexities of the artery wall poses several new conceptual and methodological challenges in the cardiovascular biomechanics. There exist several recent frameworks, in fact, to develop theories of arterial growth and remodeling (G&R) of soft tissues. Interested reader can refer to a more complete and detailed review by Humphrey and Rajagopal [38, 39] and in [41]. However, in this study, we restrict our attention to structural based formulations to emphasize their particular effects.

2.4. Geometrical model

By using Finite Element analyses, Fillinger et al. [23] showed that peak wall stress is a more reliable parameter than maximum transverse diameter in predicting potential rupture event. These findings appear to be supported by the results obtained by Venkatasubramaniam et al. [79], who indicated that the location of the maximum wall stress correlates well with the site of rupture and, additionally, by the observation that AAA formation is accompanied by an increase in wall stress [55, 83], and a decrease in wall strength [84]. Simulation on 3D patient-specific models are aimed to analyze the distribution of the wall stress to estimate the rupture risk during the evolution of the pathology [23], the effect of the thrombus [29, 85] or calcification [42, 45, 68] on the peak stress. Integration of geometry data with solid modelling is used for estimation of vessel wall distension, strain and stress patterns. Studies, to date, have typically used 3D geometries usually obtained from computer tomography (CT) [52] or MRI [7] scans or have used simplified morphologies [17, 62]. Figure 5 reports as example the phases from a CT reconstruction. However, both approaches present some limitations. In particular, it is worth pointing out that 3D simulations are not fully patient-specific models but only based on 3D patient-specific geometries while the material properties are assumed as mean population values due to the difficulty of assessing *in-vivo* material properties. Consequently, to date, no fully patient-specific model has been performed. Additionally, due to the complexity of the structure and the high computational cost required by patient-specific models, sensitivity analyses have not been performed on 3D real geometries, and only univariate investigations have been performed on idealized shapes, to estimate the influence of a single parameter on the whole stress map [63].

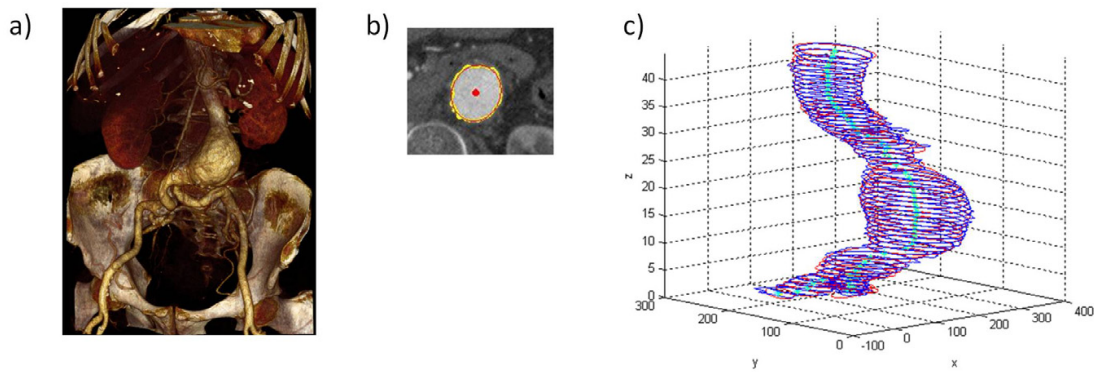


Figure 5. Example of AAA (a), segmentation of a CT cross section (b) and 3D reconstruction of a AAA (c), from [10].

3. Regional variations in wall thickness and material properties

As reported in previous section, starting from the observation that most AAAs are characterized by a complex not axisymmetric geometries a growing amount of literature has been published on the influence of the geometrical features. However one limitation in all the studies published so far is a constant wall thickness and homogeneous material assumed in the FE models.

Wall thickness. While the segmentation of the arterial lumen is a well established technique and has been performed with different modalities in living subjects, the segmentation of the wall and its connective components is not a feasible process due to the low contrast between the wall and the surrounding tissues. The conventional imaging techniques, in fact, do not provide sufficient spatial resolution to assess the wall thickness measurement and variant *in-vivo*.

During the AAA formation the artery wall is subjected to the remodelling process [77] and, as a consequence, the ratio between AA and AAA wall thickness changes. Di Martino et al. [18] noted a significant difference in wall thickness between ruptured and elective AAAs (3.6 ± 0.3 mm vs 2.5 ± 0.1 mm, respectively). By comparing the wall thickness between healthy and pathological samples, Vande Geest et al. [77] reported that the mean measured thickness values were 1.49 ± 0.11 and 1.32 ± 0.08 mm for the AA and AAA specimens, respectively. In all these studies, samples were measured only in the anterior area and consequently no information regarding regional variation between ventral and dorsal was reported. Thubrikar et al. [70] obtained five whole unruptured AAA specimens during surgical resection. Raghavan et al. [54] performed similar measures on three unruptured and one ruptured AAA, harvested as a whole during necropsy. More recently Celi et al. [10] performed measurements on 12 harvested unrupture ascending segments. In Table 1, the main results of these experimental measures are reported for both anterior and posterior region (mean \pm sd).

It is worth to notice that the thickness distribution seems to be opposite of that in the normal abdominal aorta where the wall is thicker than the posterior wall in 64% of cases [74].

From the computational point of view, in literature only few authors have investigated the effect on wall thickness reduction. Scotti et al. [67] used a non uniform wall thickness in an

N. of samples	District	$Thk_{anterior}$ (mm)	$Thk_{posterior}$ (mm)	Ref
5	AAA	2.09 ± 0.51	2.73 ± 0.46	[70]
4	AAA	2.25 ± 0.37	2.34 ± 0.48	[54]
12	aTAA	1.63 ± 0.48	2.18 ± 0.35	[10]

Table 1. Wall thickness measurements, reported in literature, categorized by circumferential location as anterior and posterior

idealized isotropic model to performed FSI simulations. Their results show that the models with a non uniform wall thickness have a maximum wall stress nearly four times that of a uniform one. Starting from experimental measurement on 12 human harvested ascending aortic samples, Celi et al. [10] developed structural 3D models of ascending AAA by including wall thickness regional variation between dorsal and ventral areas.

Material properties. As far as the material properties, to date, different behavior has funded between healthy (HAA) and pathological samples. However, due to the lack of sufficient biaxial data, a full characterization in regional variations are not provided (in circumferential direction in particular), and mechanical tests have been performed mainly in the ventral area where the bulge was formed. As well as the material properties change during the AAA progression, also the wall strength value changes. This aspect plays a fundamental role in the rupture phenomenon. In fact, the concept is that AAA rupture follows the basic principles of material failure; i.e., an aneurysm ruptures when the mural stresses or deformation meets an appropriate failure criterion. In the filed of the classical mechanics, this concept is defined by means of the potential rupture risk (RPI) parameter and quantify as the ratio of local wall stress to local wall strength:

$$RPI = \frac{\text{local stress}}{\text{local strength}} \quad (15)$$

In the same manner the safety factor (SF) can be used as the inverse of the RPI.

Thubrikar et al. [70] performed uniaxial tensile tests in both longitudinal and circumferential direction, on samples from five aneurysms. To study the regional variation they obtained samples from anterior, lateral (without distinction between left and right side) and posterior regions. In this study, however, authors did not perform tests until failure and they recorded the yield stress to define the initial point of a permanent damage. Thubrikar et al. observed that in both directions, the yield stress was greater in the lateral region with respect to the anterior and the posterior region, Figure 6(a). Experimental values regarding ultimate stress were reported by Raghavan et al. [54], Figure 6(b). They cut multiple longitudinally oriented rectangular specimen strips at various locations from three unruptured AAA and one ruptured AAA for a total of 48 strips. Samples were tested uniaxially until failure. They observed that the failure tension (ultimate) of specimen strips varied regionally from 55 kPa (near the rupture site) to 423 kPa at the undilated neck. However they report that there was no perceptible pattern in failure properties along the circumference.

Using multiple linear regression, Vande Geest et al. [78] proposed a mathematical model to estimate the wall strength by including several mixed parameters such as the gender, the presence of the intraluminal thrombus (ILT) and the family history. The final statistical model for local Cauchy wall strength (Eq. 16, dimension in kPa) was given by:

$$\sigma_u = 719 - 379 \left(ILT^{\frac{1}{2}} - 0.81 \right) - 156 (D_{NORM} - 2.46) - 213 HIST + 193 SEX \quad (16)$$

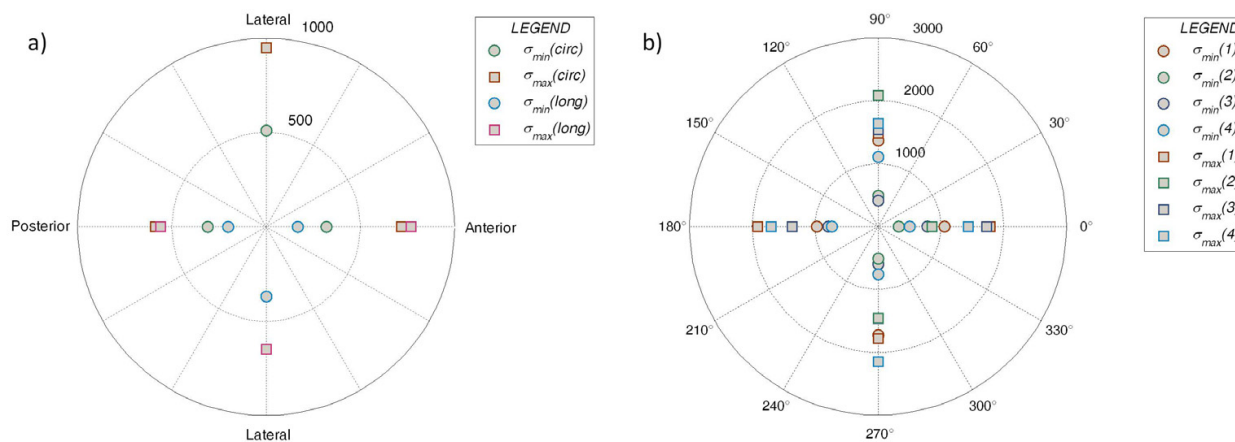


Figure 6. Yield stress in circumferential (upper side) and longitudinal (lower side) direction from [70] (a). Failure stress by circumferential location as anterior (0°), left (90°), posterior (180°) and right (270°) regions from [54] (b).

where $ILT^{\frac{1}{2}}$ is the square root of the ILT thickness whose units, D_{NORM} is a dimensionless parameter for local normalized diameter, HIST is a dimensionless binary variable ($1/2$ for positive family history, $-1/2$ for no family history), and SEX is a dimensionless binary variable for gender ($1/2$ for males, $-1/2$ for females). Table 2 depicts some examples of the effect of the coefficients of Eq. 16 by varying the gender and the ILT thickness.

Case	ILT (cm)	D_{NORM}	HIST	SEX	σ_u (kPa)
1	0	3.9	0.5	0.5	917.71
2	0	3.9	0.5	-0.5	598.35
3	1	3.9	0.5	-0.5	219.35

Table 2. Effect of the gender (case 1 vs. case 2) and of ILT thickness (case 2 vs. case 3) on the wall strength by using Eq. 16.

As we can notice the presence of the ILT decreases significantly the σ_u of about 63%. However, it is worth to notice that Eq. 16 describes local variation of the wall strength only in terms of normalized diameter and ILT thickness. Indeed Fillinger et al. [24] report that aneurysms likely rupture at stresses of 450 kPa or lower.

4. Finite element analyses

In order to get some indications on how regional variation of wall thickness and material properties affect the wall stress, two different FE models were developed. The first case describes a simplified model where an isotropic SEF has been adopted [56]. The tissue was described as homogeneous and consequently no distinction between healthy and pathological tissues was modeled. The second model introduces anisotropy and material regional variation to obtain more realistic simulations. For this last model, three different regions were considered and characterized with specific anisotropic SEFs: healthy material for the necks (HAA), pathological for the anterior bulge (AAA) and pathological for the posterior (AHA). Due to no data were available for the posterior region, a simple data manipulation was applied to define the new AHA pathological dataset starting from AAA experimental data as previously described in [9]. Figure 7 depicts the anisotropic dataset for the three

representative materials. As we can observe, the AHA dataset is able to reproduce an intermediate mechanical behavior between full healthy and pathological material.

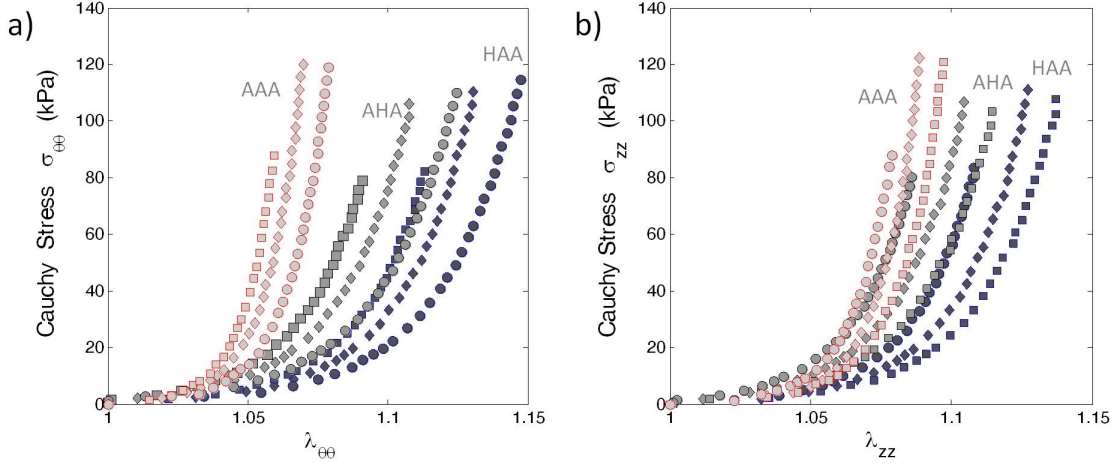


Figure 7. Example of HAA and AAA material models and virtual dataset (AHA) adopted for the transition region.

Both FE models are characterized by a wall thickness reduction in longitudinal and circumferential direction. For the necks, a wall thickness value equal to 1.8 mm was used while reduction of 30% and 50% was applied for the ventral area and of 20% for the dorsal one. Aneurysm shapes were defined as idealized 3D geometries with circular cross sections. Meridian lines describing the interior surface were based on a SZ-shaped function reported in Equation 17:

$$z(r) = \begin{cases} R_0 & 0 \leq z \leq a \\ 2(R_{AAA} - R_0) \left(\frac{z-a}{b-a} \right)^2 + R_0 & a < z \leq \frac{a+b}{2} \\ (R_{AAA} - R_0) - 2 \left(\frac{z-b}{b-a} \right)^2 + R_0 & \frac{a+b}{2} < z \leq b \\ R_{AAA} & b < z \leq \frac{L}{2} \end{cases} \quad (17)$$

where the parameter a and b locate the extremes of the slope portion of the curve. Due to symmetry only one-half of the profile is reported. Geometrical profiles are reported in Fig. 8.

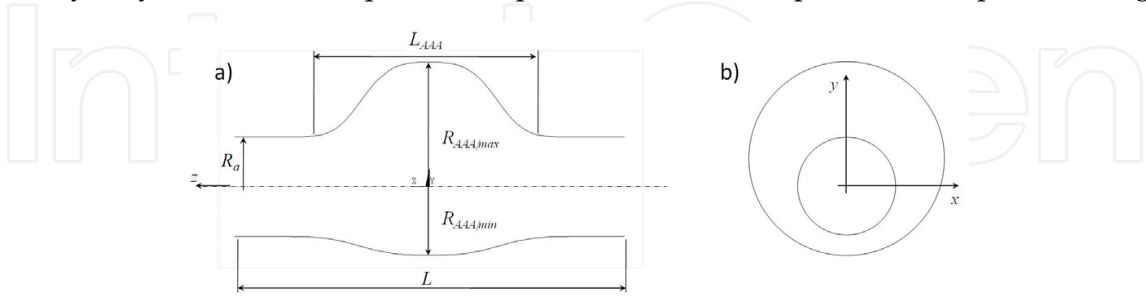


Figure 8. Lateral (a) and frontal (b) view of an asymmetrical aneurysmatic shape.

where where R_a is the radius of the healthy artery, $R_{AAA|max}$ is the maximum radius of the aneurysm in the ventral region, $R_{AAA|min}$ is the maximum radius of the aneurysm in the dorsal site. L (equal to 80 mm) defines the length of the abdominal vessel and L_{AAA} is the length of the aneurysmatic area. Figure 9(a) depicts an example of meshed asymmetric aneurysm with indication of the three anisotropic materials (in accordance with Fig. 7, while

in Figure 9(b)) transversal cross section at the maximum diameter is reported with indication of circumferential wall thickness reduction.

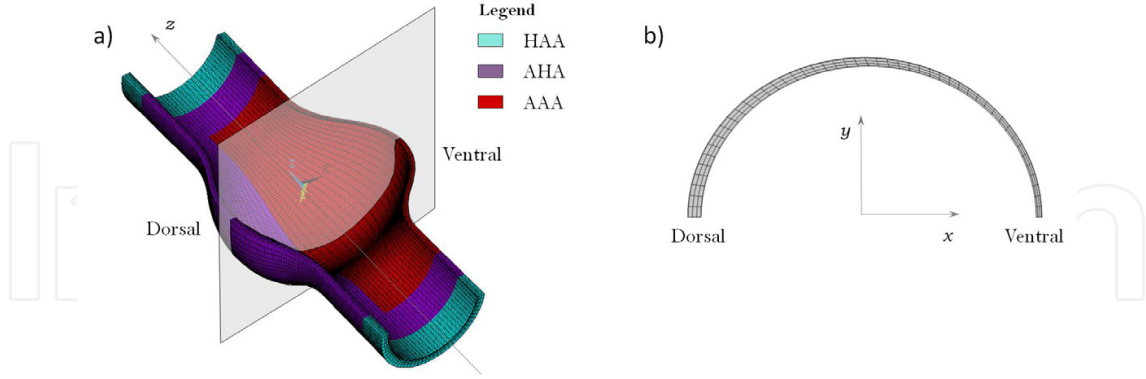


Figure 9. Example of asymmetric aneurysm and assignment of local material properties (a) and transversal cross section (b) with a wall thickness reduction of 50% and 20% in the ventral and dorsal region respectively.

For the constitutive equations for both healthy and pathological tissue, an invariant-based anisotropic polynomial SEF was chosen, as reported in Eq. 18. The material coefficients were calculated by using a specific weighted non-linear regression procedure implemented in Matlab and based on the Levenberg-Marquardt algorithm.

$$W_{isoch} = \sum_{i=1}^3 a_i (\bar{I}_1 - 3)^i + 2 \sum_{j=2}^6 b_j (\bar{I}_4 - 1)^j \quad (18)$$

Aneurysms were inflated applying a uniform inner pressure of 16 kPa, corresponding to the nominal value of peak systolic pressure. The ends of the vessels were left free to move in the radial direction.

4.1. Sensitivity analysis

To evaluate the sensitivity of the maximum stress state with respect to geometrical features, sensitivity and multivariate analyzes were also carried out by means of ANSYS Probabilistic Design Toolbox. This type of investigation presents two main advantages: the spread of the response of the output variables can be found, and it is possible to define the parameters that mainly influence the response of the system, for further details see [3, 46, 58]. Correlation coefficients are used as a measure of the strength of the relationship between input parameter and output measure.

In this study, analyzes were performed using the Monte Carlo method, in which the correlations between input and output variables are defined in a completely statistical way. In order to reduce the number of samples, the Latin Hypercube technique, instead of a direct sampling, was adopted. The effectiveness of these procedures was previously tested by Celi [8] and Celi et al. [11]. In order to study the effect of the AAA geometry on the distribution of the wall stresses, we introduced three dimensionless geometrical parameters:

$$F_R = \frac{R_{AAA}}{R_a}; \quad F_L = \frac{L_{AAA}}{R_{AAA}}; \quad F_{sym} = \frac{R_{AAA|min} - R_a}{R_{AAA|max} - R_a}; \quad F_{thk} = \frac{thk_0 - thk_{min}}{thk_0} 100 \quad (19)$$

The parameter F_R defines the ratio between the maximum AAA radius and the healthy arterial radius, F_L defines the ratio between the length of the aneurysm and the maximum AAA radius, while $F_{sym} \in [0,1]$ is a measure of the aneurysmal eccentricity. The extreme cases $F_{sym}=1$ and $F_{sym}=0$ define the symmetrical situation and the most asymmetric geometry, respectively. Table 3 summarizes the FE analyses performed in this study.

Parameter	Definition	Distribution	Range
F_R	Dilatation ratio	uniform	1.5-3
F_L	Shape factor	uniform	1.5-4
F_{sym}	Symmetry factor	uniform	0-1
F_{thk}	Thickness ratio	uniform	0-50

Table 3. Range of the geometric parameters defining the aneurysmal shape.

Model	Thk	N. of materials	Type of Material	Type of Analysis
Iso ₁	variable	1 (AAA)	Iso	Det./Prob.
Aniso ₁	variable	1 (AAA)	Aniso	Det.
Aniso ₃	variable	3 (AAA, AHA, HAA)	Aniso	Det.

Table 4. Scheme of the simulations performed in this study.

4.2. Results

Fitting procedure. The results of the best fit procedures for the anisotropic SEFs are reported in Figure 10. For all models very good results were obtained and, as a metric of the goodness of fit, the root mean square of the fitting error were computed: $R^2=0.992$, $R^2=0.992$ and $R^2=0.983$ from healthy to pathological tissue, respectively.

Table 5 lists the parameters values for the HAA, AHA and AAA models. The angle θ represents the embedded fiber orientations, as illustrated in Fig. 4(a).

Model	a_1	a_3	a_3	b_4	b_5	b_6	θ	R^2
HAA	2.503	1.641	896.714	3.467	1.564	102.677	45.510	0.992
AHA	12.194	40.869	2166.994	2.483	41.883	64.650	52.199	0.992
AAA	1.5	0.1	4966.781	54.381	3856.291	4997.367	45.989	0.983

Table 5. Coefficients for the models for the three SEFs. Vales in kPa

Thus, the new models adequately reproduce the experimental data sets for HAA, AHA and AAA tissues using only one SEF with six parameters per model. Figure 10(c-f-i) points out the changes in the anisotropic effect by increasing the pathological response of a tissue from healthy to aneurysmatic state.

FE simulations. Distributions of the circumferential stresses for the isotropic and anisotropic models for three different values of F_{thk} are shown in Fig. 11. It can be observed that for all models and geometries, the maximum stress is localized in the interior wall surface and in the proximity of the minor radius of curvature, due to the geometrical effect of the curvature itself, and that there exists a stress gradient through the aneurysm wall thickness. As expected, the isotropic model underestimates the peak stress value of about 40%, 38%, 42% with respect to the 2FF homogeneous anisotropic model, Fig. 11(d-e-f), of about 44%, 40%, 43% with respect to the 2FF heterogeneous model, Fig. 11(g-h-i). By focusing our attention on the anisotropic

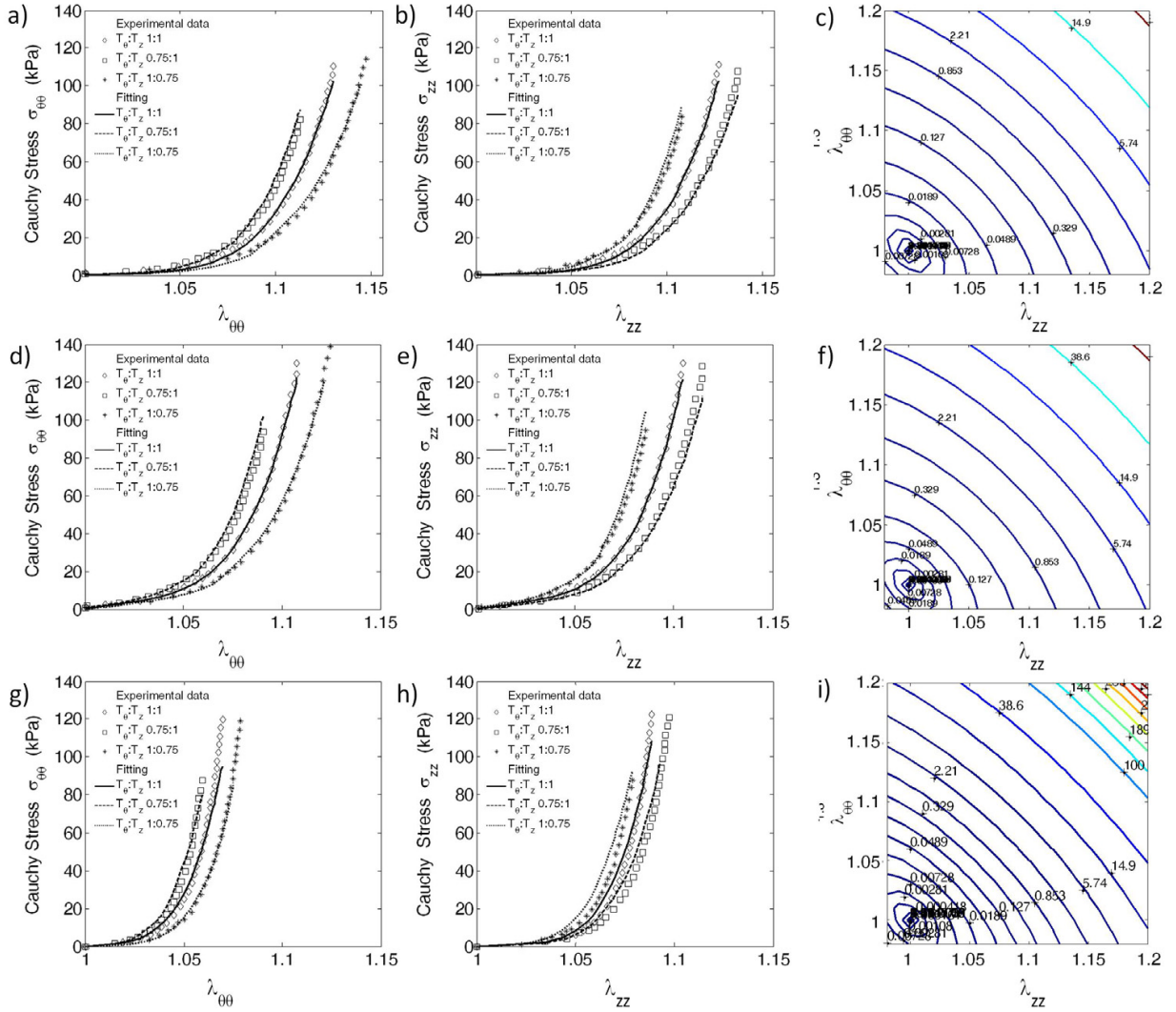


Figure 10. Representative stress-stretch data and fitting results for an HAA (a-b), AHA (d-e) and AAA (g-h) in circumferential and axial direction, see Fig. 7. The isolines of the SEFs for all models are reported in (c), (f) and (i).

models, as we can observe, the 2FF heterogeneous models present the highest maximum stress values due to the presence of the additional two material (HAA and AHA). The effect of these materials is to increase deformation in both radial and axial directions of the ventral and dorsal regions by changing, as a consequence, the local curvature.

As far as the stress gradient, Figure 12 depicts the transmural circumferential stress for model $Aniso_1$ and $Aniso_3$ for the two extreme cases of constant wall thickness and of maximum reduction. In the bulge area, Fig. 12(a), models $Aniso_1$ and $Aniso_3$ present the same stress gradient behavior due to the use of the same material (AAA). The effect of the wall thickness reduction is an increase of about 30% in the bulge region where the maximum diameter is reached. In the dorsal region, Fig. 12(b) the wall thickness reduction increases the maximum stress of about 8% for both models, while, the combined effect of the wall thickness reduction and different material produces an increase of about 21%. As far as the multivariate analysis, under the assumption of a constant wall thickness, the peak stress, is primarily affected by F_R , while if the wall thickness reduction in the bulge (F_{thk}) is considered, F_{thk} plays the main role.

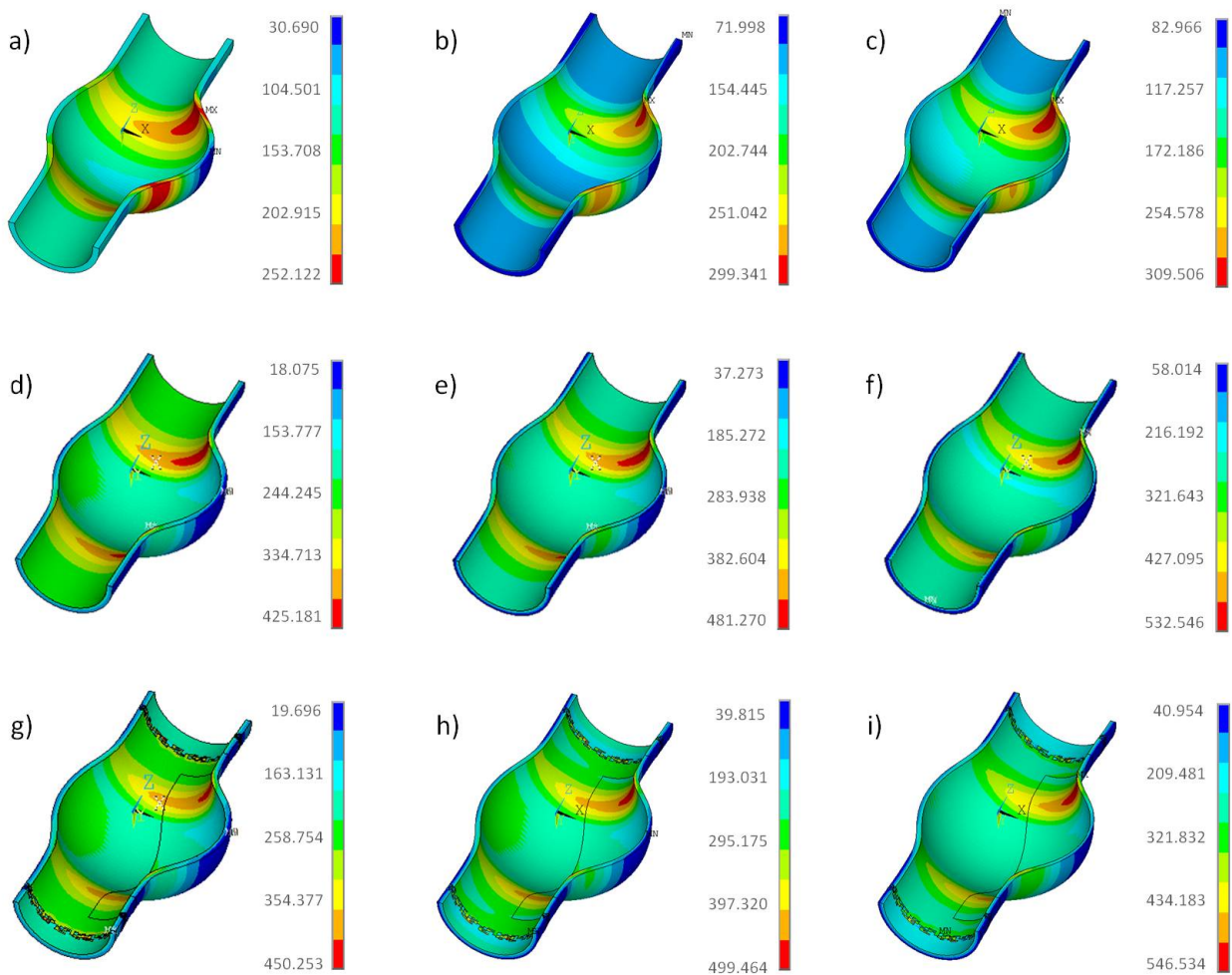


Figure 11. Contour plots of the circumferential stress for model Iso₁ (a-c), Aniso₁ (d-f) and Aniso₃ (g-i) with progressive wall thickness reduction. Constant wall *thk* (a,d,g), reduction of 30% and 20% (b,e,h) and reduction of 50% and 20% (c,f,i) in ventral and dorsal area. Stress in kPa.

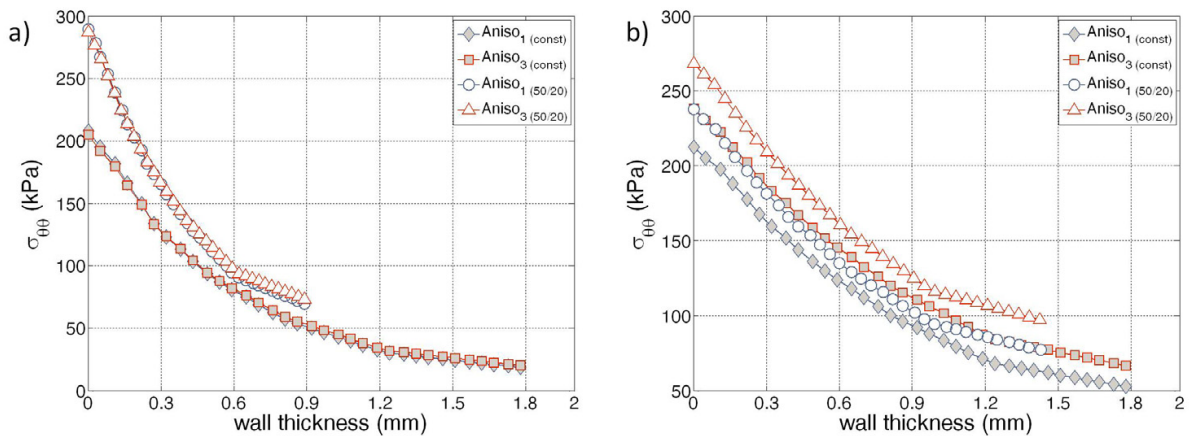


Figure 12. Stress gradient (kPa) in the ventral (a) and dorsal (b) area for the anisotropic models by considering constant wall thickness and the reduction of 50% and 20% in ventral and dorsal area.

Moreover, the same stress value is obtained both in fusiform aneurysm with critical dimension ($F_{thk} \simeq 2.5$) and in saccular with $F_{thk} \simeq 2$, see Figure 13(a). Including the wall thickness variation in the multivariate analyses points out the importance of these parameters. Figure 13(b) depicts the correlation coefficients (C.C.) for each input variable: the stresses increase as the diameter increases, but decrease as the thickness increases. Additionally, shorter models had higher wall stress.

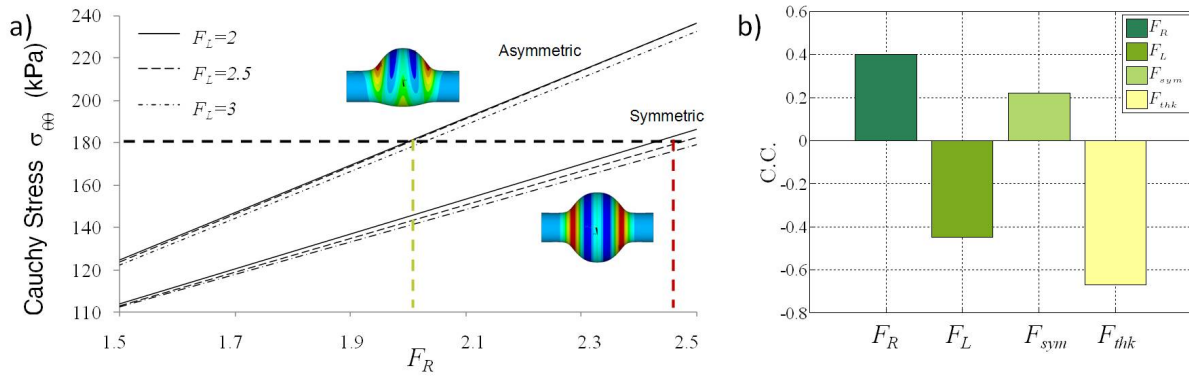


Figure 13. Maximum circumferential stresses as a function of F_R and F_L parameters (a) and correlation coefficients (C.C.) for each geometrical parameters (b).

5. Discussion and conclusion

In the first part of this work a literature survey on AAA biomechanics is reported by including several aspects from experimental test to constitutive model formulations. In the second part our FE models are presented, aimed at simulating and enhancing the computational study of the aneurismatic pathology. With respect to previous works, a more realistic type of AAA, even if idealized, was considered defined by means of regional variation of wall thickness and material properties. Notwithstanding many important findings from prior finite element stress analyses, all models are limited by the assumption of material homogeneity and constant wall thickness, e.g. [17, 55, 59, 62, 63]. Starting from the principle that intramural cells seek to remodel the arterial wall in order to maintain and to restore stresses towards homeostatic values, the material and geometrical properties must vary from region to region. This concept is the base of the remodeling phenomena as suggest by Humphrey [37]. In order to include material regional variation, in this work, we have introduced a simplified form of the stored energy function (Equation 18), motivated directly by microstructural information on two collagen fiber families [66]. This constitutive form fits well (e.g. mean R^2 of about 0.9) healthy and pathological available human biaxial data without complexity. Our SEF, in fact, is able to cope the progressive decrease in the elastin contribute (associated with the isotropic contribution attributed to an elastin-dominated amorphous matrix [34]) and increase in the anisotropic effects (associated with the predominant families of collagen fibers). The decrease of the elastin from heathy to pathological state as well as the increase of anisotropy are reported in Figure 14 where the isotropic (W_{iso}) and anisotropic (W_{aniso}) components of the SEF for HAA and AAA models are reported.

The present nonlinear regression focused not only on the estimating global best-fit values of model parameters suitable for performing stress analyses, but also on their effect in terms of energy behavior and changes from heathy to pathological tissue (Figure 10(c-i)). In

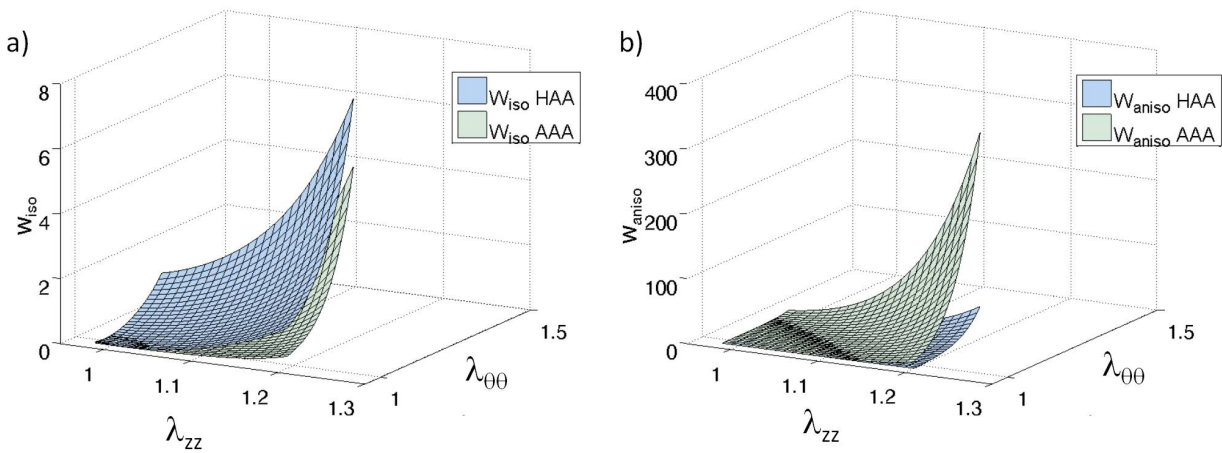


Figure 14. Isotropic (a) and anisotropic (b) component of the SEF reported in Eq. 18 for healthy (HAA) and pathological (AAA) tissue.

parallel to the marked decrease in the isotropic stored energy for AAA tissues (as describe above), we can observed an increase of stiffness capturing the observed biaxial reduction in extensibility/distensibility in particular in the circumferential direction (see Fig. 10(g)). As mention in Sec. 1, in current clinical practise, the aortic diameter is the main feature that is used to predict the risk of rupture. The more reliable quantification of the rupture risk is provided by the RPI parameter of Eq. 15 (and similar), however, which stress (principal stress, circumferential stress or von Mises stress) and strength is still matter of controversy. Gaining an understanding of the mechanical properties of the AAA tissue therefore is of clinical significance. Due to the difficult to reliably predict abdominal aortic aneurysm expansion and rupture in individuals several clinical trials have been performed [25, 72]. At the same time, from the computational point of view, literature systematically reports the evidence to support the role of patient-specific biomechanical profiles in the management of patients with AAA both from imaging and FE approach [1, 13, 81]. In order to accurately predict the risk of rupture of AAA, is necessary to predict the AAA wall strength distribution and the material properties non-invasively. With regard to our work, our specific FE simulations (both deterministic and probabilistic), reveal the importance to define a more realistic geometrical shape by including also wall thickness regional variation. Several previous studies were devoted to the definition of the geometrical parameters that mainly influence the wall stress (Vorp et al. [83] and more recently Rodríguez et al. [62] found that wall stress is substantially increased by an asymmetric bulge in AAAs, just to cite but a few), but, to the best of our knowledge, this is the first structural study in which also the wall thickness is considered as variable. Figure 15 depicts results from two deterministic simulations extracted by the multivariate analysis: aneurysm with a large diameter and constant wall thickness (a) and FE model small diameter and a wall thickness reduction of 50% in the ventral area. The stress contour plot points out how the wall thickness reduction influence the maximum stress value and its localization.

To conclude, there is, therefore, a pressing need to include patient specific regional variations to identify regions within AAAs that have the highest ratio of stress to strength. Future studies on patient-specific geometries of AAAs should consider the actual wall thickness. Moreover, the understanding the mechanical properties of the AAA wall will enhance our ability to design implants that can stay in place and/or protect the aneurysm wall from blood pressure.

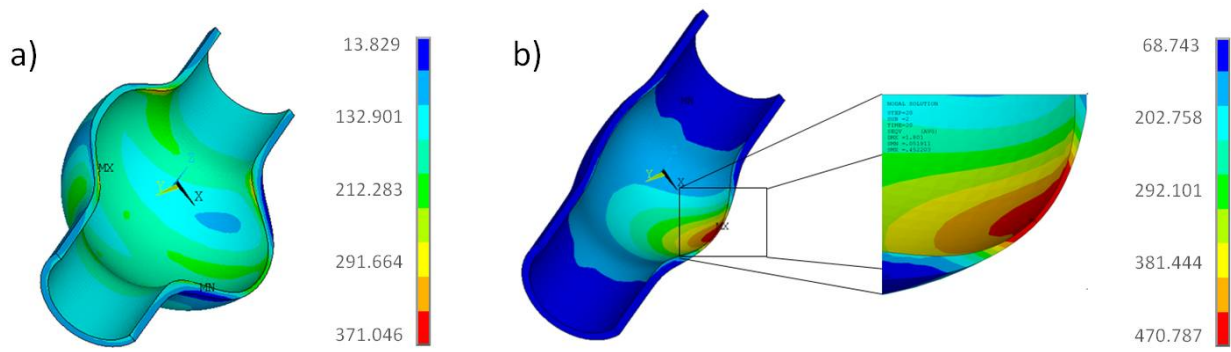


Figure 15. Stress contour plot of aneurysm with a large diameter and constant wall thickness (a) and a FE model small diameter and a wall thickness reduction of 50% in the ventral area.

Author details

Simona Celi

*Institute of Clinical Physiology National Research Council IFC-CNR, Massa
Fondazione Toscana CNR "G. Monasterio", Heart Hospital, Massa, Italy*

Sergio Berti

Fondazione Toscana CNR "G. Monasterio", Heart Hospital, Massa, Italy

6. References

- [1] Abbas, A., Attia, R., Smith, A. & M.Waltham [2011]. Can we predict abdominal aortic aneurysm (aaa) progression and rupture by non-invasive imaging?-a systematic review, *International Journal of Clinical Medicine* 2: 484–499.
- [2] Alexander, J. J. [2004]. The pathobiology of aortic aneurysms, *Journal of Surgical Research* 117: 163–175.
- [3] Ang, A. S. & Tang, W. H. [1984]. *Probabilistic concepts in engineering planning and design, Decision, risk and reliability*, John Wiley & Sons Inc.
- [4] Baek, S., Gleason, R., Rajagopal, K. & Humphrey, J. [2007]. Theory of small on large: Potential utility in computations of fluid–solid interactions in arteries, *Computer Methods in Applied Mechanics and Engineering* 196: 3070–3078.
- [5] Basciano, C. A. & Kleinstreuer, C. [2009]. Invariant-based anisotropic constitutive models of the healthy and aneurysmal abdominal aortic wall, *Journal of Biomechanical Engineering* 131(2): 021009 (11 pages).
- [6] Boehler, J. P. [1987]. *Introduction to the Invariant Formulation of Anisotropic Constitutive Equations*, Springer-Verlag, Wien,, chapter Applications of Tensor Functions in Solid Mechanics, CISM Courses and Lectures No., 292, pp. 13–30.
- [7] Borghi, A., Wood, N., Mohiaddin, R. & Xu, X. [2006]. 3d geometric reconstruction of thoracic aortic aneurysms, *BioMedical Engineering OnLine* 5(59): 1–13.
- [8] Celi, S. [2012]. Numerical and experimental simulations of surgical procedures, *PhD Thesis*, University of Pisa.
- [9] Celi, S. & Berti, S. [2012]. FE simulations on the effect of regional variations of material properties and wall thickness on AAA, *GNB congress*, ISBN: 978 88 555 3182-5.

- [10] Celi, S., Berti, S., Mariani, M., Di Puccio, F. & Forte, P. [2010]. Investigation on the effect of the wall thickness in rupture risk estimation of aaa by a probabilistic finite element approach, *European Heart Journal* 31 (Supp)(1): 284.
- [11] Celi, S., Di Puccio, F. & Forte, P. [2011]. Advances in finite element simulations of elastosonography for breast lesion detection, *Journal of Biomechanical Engineering* 133: 081006–13.
- [12] Choi, H. S. & Vito, R. P. [1990]. Two-dimensional stress-strain relationship for canine pericardium, *Journal of Biomechanical Engineering* 112(2): 153–159.
- [13] Choke, E., Cockerill, G., Wilson, W., Sayed, S., Dawson, J., Loftus, I. & Thompson, M. [2005]. A review of biological factors implicated in abdominal aortic aneurysm rupture, *European Journal of Vascular and Endovascular Surgery* 30(3): 227–244.
- [14] Chuong, C. J. & Fung, Y. C. [1983]. Three-dimensional stress distribution in arteries, *Journal of Biomechanical Engineering* 105(3): 268–274.
- [15] Cox, R. [1978]. Regional variation of series elasticity in canine arterial smooth muscles., *American Journal of Physiology* 234(5): H542–51.
- [16] Darling, R., Messina, C., Brewster, D. & Ottinger, L. [1977]. Autopsy study of unoperated abdominal aortic aneurysms, *Circulation* 56: 161–164.
- [17] Di Achille, P., Celi, S., Di Puccio, F. & Forte, P. [2011]. Anisotropic aaa: computational comparison between four and two fiber family material models, *Journal of Biomechanics* 44(13): 2418–26.
- [18] Di Martino, E., Bohra, A., Geest, J. V., Gupta, N. & Vorp, M. M. D. [2006]. Biomechanical properties of ruptured versus electively repaired abdominal aortic aneurysm wall tissue, *Journal of Vascular Surgery* 43(3): 570–576.
- [19] Di Puccio, F., Celi, S. & Forte, P. [2012]. Review of experimental investigations on compressibility of arteries and the introduction of a new apparatus, *Experimental Mechanics* 52(7): 1–8, DOI: 10.1007/s11340-012-9614-4.
- [20] Dingemans, K., Teeling, P., Lagendijk, J. & Becker, A. [2000]. Extracellular matrix of the human aortic media: an ultrastructural histochemical and immunohistochemical study of the adult aortic media, *The Anatomical Record* 258(1): 1–14.
- [21] Dobrin, P. [1989]. Pathophysiology and pathogenesis of aortic aneurysms. current concepts, *Surgical Clinics of North America Journal* 69(4): 687–703.
- [22] Ferruzzi, J., Vorp, D. A. & Humphrey, J. D. [2011]. On constitutive descriptors of the biaxial mechanical behaviour of human abdominal aorta and aneurysms, *Journal of the Royal Society Interface* 8: 435–450.
- [23] Fillinger, M. F., Marra, S. P., Raghavan, M. L. & Kennedy, F. E. [2003]. Prediction of rupture risk in abdominal aortic aneurysm during observation: wall stress versus diameter, *Journal of Vascular Surgery* 37: 724–732.
- [24] Fillinger, M. F., Raghavan, M. L., Marra, S. P., C., J. L. & Kennedy, F. E. [2002]. In vivo analysis of mechanical wall stress and abdominal aortic aneurysm rupture risk, *Journal of Vascular Surgery* 36(3): 589–597.
- [25] Fleming, C., Whitlock, E. P., Beil, T. L. & Lederle, F. A. [2005]. Screening for abdominal aortic aneurysm: A best-evidence systematic review for the u.s. preventive services task force, *Annals of Internal Medicine* 142(3): 203–211.
- [26] Fung, Y. C., Fronek, K. & Patitucci, P. [1979]. Pseudoelasticity of arteries and the choice of its mathematical expression, *American Journal of Physiology* 237(5): AH620–31.
- [27] Ganten, M. K., Krautter, U., von Tengg-Kobligk, H., H., D. B., Schumacher, Stiller, W., Delorme, S., Kauczor, H., Kauffmann, G. & Bock, M. [2008]. Quantification of aortic

- distensibility in abdominal aortic aneurysm using ecg-gated multi-detector computed tomography, *Vascular-Interventional* 18(5): 966–73.
- [28] Gasser, T. C. [2011]. An irreversible constitutive model for fibrous biological tissue: a 3d microfiber approach with demonstrative application to abdominal aortic aneurysms, *Acta Biomaterialia* 7(6): 2457–2466.
- [29] Gasser, T. C., Auer, M., Labruto, F., Roy, J. & Swedenborg, J. [2009]. Using finite element analysis to assess rupture risk in abdominal aortic aneurysms including the effect of the intraluminal thrombus., *Journal of Vascular Surgery* 49(5): S29.
- [30] Greenwald, S. E. [2007]. Ageing of the conduit arteries, *Journal of Pathology* 211: 157–172.
- [31] Haskett, D., Johnson, G., Zhou, A., Utzinger, U. & Vande Geest, J. [2010]. Microstructural and biomechanical alterations of the human aorta as a function of age and location, *Biomechanics and Modeling in Mechanobiology* 9: 725–736. 10.1007/s10237-010-0209-7.
- [32] He, C. M. & Roach, M. [1994]. The composition and mechanical properties of abdominal aortic aneurysms, *Journal of Vascular Surgery* 20(1): 6–13.
- [33] Holzapfel, G. A. [2000]. *Holzapfel, G. A., 2000, Nonlinear Solid Mechanics: A Continuum Approach for Engineering, Wiley, England, Wiley, England.*
- [34] Holzapfel, G. A., Gasser, T. C. & Ogden, R. W. [2000]. A new constitutive framework for arterial wall mechanics and a comparative study of material models, *Journal of Elasticity* 61: 1–48.
- [35] Holzapfel, G. A., Gasser, T. C. & Stadler, M. [2002]. A structural model for the viscoelastic behavior of arterial walls: continuum formulation and finite element analysis, *European Journal of Mechanics–A/Solids* 21(3): 441–463.
- [36] Humphrey, J. D. [1995]. Mechanics of the arterial wall: review and directions, *Critical reviews in biomedical engineering* 23(1/2): 1–162.
- [37] Humphrey, J. D. [2008]. Vascular adaptation and mechanical homeostasis at tissue, cellular, and sub-cellular levels, *Cell Biochem. Biophys.* 50: 53–78.
- [38] Humphrey, J. D. & Rajagopal, K. R. [2002]. A constrained mixture model for growth and remodeling of soft tissues, *Mathematical Models and Methods in Applied Sciences* 12: 407–430.
- [39] Humphrey, J. D. & Rajagopal, K. R. [2003]. A constrained mixture model for arterial adaptations to a sustained step change in blood flow, *Biomech Model Mechanobiol* 2(2): 109–26.
- [40] Humphrey, J. D. & Yin, F. C. [1987]. A new constitutive formulation for characterizing the mechanical behavior of soft tissues, *Biophysical Journal* 52(4): 563–570.
- [41] Kuhl, E. & Holzapfel, G. A. [2007]. A continuum model for remodeling in living structures, *Journal of Materials Science* 42: 8811–8823.
- [42] Li, Z.-Y., Sadat, U., U-King-Im, J., Tang, T. Y., Bowden, D. J., Hayes, P. D. & Gillard, J. H. [2010]. Association between aneurysm shoulder stress and abdominal aortic aneurysm expansion. a longitudinal follow-up study, *Circulation* 122: 1815–1822.
- [43] Länne, T., Sonesson, B., Bergqvist, D., Bengtsson, H. & Gustafsson, D. [1992]. Diameter and compliance in the male human abdominal aorta: influence of age and aortic aneurysm, *European Journal of Vascular Surgery* 6(2): 178–184.
- [44] MacSweeney, S. T., Young, G., Greenhalgh, R. M. & Powell, J. T. [1992]. Mechanical properties of the aneurysmal aorta, *British Journal of Surgery* 79(12): 1281–4.
- [45] Maier, A., Gee, M. W., Reeps, C., Eckstein, H. H. & Wall, W. A. [2010]. Impact of calcifications on patient-specific wall stress analysis of abdominal aortic aneurysms., *Biomech. Model. Mechanobiol.* 9(5): 511–21.

- [46] McKay, M. D., Beckman, R. J. & Conover, W. J. [1979]. A comparison of three methods for selecting values of input variables in the analysis of output from a computer code, *Technometrics* 42: 55–61.
- [47] Molacek, J., Baxa, J., Houdek, K., Treska, V. & Ferda, J. [2011]. Assessment of abdominal aortic aneurysm wall distensibility with electrocardiography-gated computed tomography, *Annals of Vascular Surgery* 25(8): 1036–1042.
- [48] Murphy, S. L., Xu, J. & Kochanek, K. D. [2012]. Deaths: Preliminary data for 2010, *National Vital Statistics System* 60(4): 1–68.
- [49] Nichols, W. W. & O'Rourke, M. [1997]. *McDonald's Blood Flow in Arteries: Theoretical, Experimental and Clinical Principles (4th ed.)*, Hodder Arnold Publication.
- [50] Ogden, R. W. [2009]. Anisotropy and nonlinear elasticity in arterial wall mechanics, in G. A. Holzapfel, R. W. Ogden, F. Pfeiffer, F. G. Rammerstorfer, J. Salençon, B. Schrefler & P. Serafini (eds), *Biomechanical Modelling at the Molecular, Cellular and Tissue Levels*, Vol. 508 of *CISM Courses and Lectures*, Springer Vienna, pp. 179–258.
- [51] O'Rourke, M. F. & Hashimoto, J. [2007]. Mechanical factors in arterial aging: A clinical perspective, *Journal of the American College of Cardiology* 50: 1–13.
- [52] Polzer, S., Gasser, T., Swedenborg, J. & Bursa, J. [2011]. The impact of intraluminal thrombus failure on the mechanical stress in the wall of abdominal aortic aneurysms, *European Journal of Vascular and Endovascular Surgery* 41(4): 467–473.
- [53] Raghavan, M. L. & da Silva, E. S. [2011]. *Studies in Mechanobiology, Tissue Engineering and Biomaterials*, Springer, chapter Mechanical Properties of AAA Tissue, pp. 139–162.
- [54] Raghavan, M. L., Kratzberg, J., de Tolosa, E. M. C., Hanaoka, M. M., Walker, P. & da Silva, E. S. [2006]. Regional distribution of wall thickness and failure properties of human abdominal aortic aneurysm, *Journal of Biomechanics* 39: 3010–3016.
- [55] Raghavan, M. L., Vorp, D. A., Federle, M. P., Makaroun, M. S. & Webster, M. W. [2000]. Wall stress distribution on three-dimensionally reconstructed models of human abdominal aortic aneurysm, *Journal of Vascular Surgery* 31: 760–769.
- [56] Raghavan, M. & Vorp, D. [2000]. Toward a biomechanical tool to evaluate rupture potential of abdominal aortic aneurysm: identification of a finite strain constitutive model and evaluation of its applicability, *Journal of Biomechanics* 33(4): 475–82.
- [57] Raghavan, M., Webster, M. & Vorp, D. [1996]. Ex vivo biomechanical behavior of abdominal aortic aneurysm: assessment using a new mathematical model, *Ann. Biomed. Eng* 24(5): 573–582.
- [58] Reh, S., Beley, J.-D., Mukherjee, S. & Khor, E. H. [2006]. Probabilistic finite element analysis using ansys, *Structural Safety* 28: 17–43.
- [59] Rissland, P., Alemu, Y., Einav, S., Ricotta, J. & Bluestein, D. . [2009]. Abdominal aortic aneurysm risk of rupture: patientspecific fsi simulations using anisotropic model, *Journal of Biomechanical Engineering* 131(3): 031001.
- [60] Rizzo, R. J., McCarthy, W. J., Dixit, S. N., Lilly, M. P., Shively, V. P., Flinn, W. R. & Yao, J. S. T. [1989]. Collagen types and matrix protein content in human abdominal aortic aneurysms, *Journal of Vascular Surgery* 10: 365–373.
- [61] Roach, M. R. & Burton, A. C. [1957]. The reason for the shape of the distensibility curves of arteries, *Canadian Journal of Biochemistry and Physiology* 35(8): 681–690.
- [62] Rodríguez, J. F., Ruiz, C., Doblaré, M. & Holzapfel, G. A. [2008]. Mechanical stresses in abdominal aortic aneurysms: influence of diameter, asymmetry, and material anisotropy, *Journal of Biomechanical Engineering* 130(2): 021023.

- [63] Rodríguez, J., Martufi, G., Doblaré, M. & Finol, E. [2009]. The effect of material model formulation in the stress analysis of abdominal aortic aneurysms, *Annals of Biomedical Engineering* 37: 2218–2221.
- [64] Sacks, M. [2000]. Biaxial mechanical evaluation of planar biological materials, *Journal of Elasticity* 61(3): 199–246.
- [65] Sakalihasan, N., Limet, R. & Defawe, O. [2005]. Abdominal aortic aneurysm, *Lancet* 365(9470): 1577–1589.
- [66] Schriefl, A. J., Zeindlinger, G., Pierce, D. M., Regitnig, P. & Holzapfel, G. A. [2011]. Determination of the layer-specific distributed collagen fibre orientations in human thoracic and abdominal aortas and common iliac arteries, *Journal of The Royal Society Interface* doi:10.1098/rsif.2011.0727: on line.
- [67] Scotti, C. M., Jimenez, J., Muluk, S. C. & Finol, E. A. [2008]. Wall stress and flow dynamics in abdominal aortic aneurysms: finite element analysis vs. fluid-structure interaction, *Computer Methods in Biomechanics and Biomedical Engineering* 11: 301–322.
- [68] Speelman, L. A., Bohra, A., Bosboom, E. M. H., Schurink, G. W. H., van de Vosse, F. N., Makaroun, M. S. & Vorp, D. A. [2007]. Effects of wall calcifications in patient-specific wall stress analyses of abdominal aortic aneurysms., *Journal of Biomechanical Engineering* 129(1): 105–109.
- [69] Spencer, A. J. M. [1984]. *Continuum Theory of the Mechanics of Fibre-Reinforced Composites*, Springer-Verlag, chapter Continuum Theory of the Mechanics of Fibre-Reinforced Composites, CISM Courses and Lectures No. 282, pp. 1–32.
- [70] Thubrikar, M., Labrosse, M., Robicsek, F., Al-Soudi, J. & Fowler, B. [2001]. Mechanical properties of abdominal aortic aneurysm wall, *Journal of Medical Engineering & Technology* 25(4): 133–42.
- [71] United Kingdom EVAR Trial Investigators, Greenhalgh, R., Brown, L., Powell, J., Thompson, S., Epstein, D. & Sculpher, M. [2010]. Endovascular versus open repair of abdominal aortic aneurysm, *New England Journal of Medicine* 362: 1863–1871.
- [72] U.S. Preventive Services Task Force [2005]. Screening for abdominal aortic aneurysm: Recommendation statement, *Annals of Internal Medicine* 142(3): 198–202.
- [73] Vaishnav, R. N., Young, J. T., Janicki, J. S. & Patel, J. S. [1972]. Non linear anisotropic elastic properties of the canine aorta, *Biophysical Journal* 12(8): 1008–1027.
- [74] Valenta, J. [1993]. *Clinical Aspects of Biomedicine*, Elsevier.
- [75] van St Veer, M., Buth, J., Merckx, M., Tonino, P., van den Bosch, H., Pijls, N. & van de Vosse, F. [2008]. Biomechanical properties of abdominal aortic aneurysms assessed by simultaneously measured pressure and volume changes in humans, *Journal of Vascular Surgery* 48(6): 1401–1407.
- [76] Vande Geest, J. P., Sacks, M. S. & Vorp, D. A. [2004]. Age dependency of the biaxial biomechanical behavior of human abdominal aorta, *Journal of Biomechanical Engineering* 12: 815–822.
- [77] Vande Geest, J. P., Sacks, M. S. & Vorp, D. A. [2006]. The effects of aneurysm on the biaxial mechanical behavior of human abdominal aorta, *Journal of Biomechanics* 39: 1324–1334.
- [78] Vande Geest, J. P., Wang, D. H. J., Wisniewski, S. R., Makaroun, M. S. & Vorp, D. A. [2006]. Towards a noninvasive method for determination of patient-specific wall strength distribution in abdominal aortic aneurysms, *Ann. Biomed. Eng.* 34(7): 1098–1106.
- [79] Venkatasubramaniam, A., Fagan, M., Mehta, T., Mylankal, K., Ray, B., Kuhan, G., Chetter, I. & McCollum, P. [2004]. A comparative study of aortic wall stress using finite element

- analysis for ruptured and non-ruptured abdominal aortic aneurysms, *European Journal of Vascular Surgery* 28: 168–176.
- [80] Vito, R. P. & Dixon, S. A. [2003]. Blood vessel constitutive models: 1995–2002, *Annu. Rev. Biomed. Eng.* 5(No. 0): 413–439.
- [81] Vorp, D. A. [2007]. Biomechanics of abdominal aortic aneurysm, *Journal of Biomechanics* 40: 1887–1902.
- [82] Vorp, D. A., Raghavan, M. L., Muluk, S. C., Makaroun, M. S., Steed, D. L., Shapiro, R. & Webster, M. W. [1996]. Wall strength and stiffness of aneurysmal and nonaneurysmal abdominal aorta, *Annals of the New York Academy of Sciences* 800(1): 274–276.
- [83] Vorp, D. A., Raghavan, M. L. & Webster, M. W. [1998]. Mechanical wall stress in abdominal aortic aneurysm: influence of diameter and asymmetry, *Journal of Vascular Surgery* 27: 632–639.
- [84] Vorp, D., Lee, P., Wang, D., Makaroun, M., Nemoto, E., Ogawa, S. & MW., M. W. [2001]. Association of intraluminal thrombus in abdominal aortic aneurysm with local hypoxia and wall weakening, *Journal of Vascular Surgery* 34: 291–9.
- [85] Wang, D. H. J., Makaroun, M. S., Webster, M. W. & Vorp, D. A. [2002]. Effect of intraluminal thrombus on wall stress in patient-specific models of abdominal aortic aneurysm, *Journal of Vascular Surgery* 36: 598–604.
- [86] Wicker, B. K., Hutchens, H. P., Wu, Q., Yeh, A. T. & Humphrey, J. D. [2008]. Normal basilar artery structure and biaxial mechanical behaviour, *Computer Methods in Biomechanics and Biomedical Engineering* 11: 539–551.
- [87] Zeinali-Davarani, S., Choi, J. & Baek, S. [2009]. On parameter estimation for biaxial mechanical behavior of arteries, *Journal of Biomechanics* 42: 524–530.